Verification of a Dual Scale Model for Sub-Filter Shear-Induced Velocities with a Vortex Sheet Method

A. Goodrich, and M. Herrmann School for Engineering of Matter, Transport and Energy Arizona State University Tempe, AZ 85287 USA

Abstract

A method to predict sub-filter shear-induced velocities on a liquid-gas phase interface for use in a dual scale LES model is presented and compared against prior work on Vortex Sheet methods. The method reconstructs the sub-filter velocity field in the vicinity of the interface by employing a vortex sheet at the interface location. The vortex sheet is transported by an unsplit geometric volume and surface area advection scheme with a Piecewise Linear Interface Construction (PLIC) representation of the material interface. At each step, the vorticity field is constructed by evaluating a volume integral of the vortex sheet and a numerical spreading parameter near the liquid-gas interface. A Poisson equation can then be constructed and solved for the vector potential; the self-induced velocities due to the vortex sheet are subsequently evaluated from the vector potential. The described vortex sheet method is tested and compared against prior literature.

 $^{{\}rm *Corresponding\ Author:\ Austin.Goodrich@asu.edu}$

Introduction

Liquid atomization is an important process occurring in many engineering applications. Internal combustion engines depend on the rapid atomization and evaporation of fuels to quickly and efficiently mix with air before combustion can occur. Evaporation of a liquid fuel is a slow process, but can be greatly enhanced by increasing the surface area of the liquid fuel. Since the residence time in combustion engines is small, the liquid fuel must be rapidly atomized into many small drops to provide a large surface area and increase the rate of evaporation. Many modern engines rely on the fuel injector design to generate the required turbulence to rapidly atomize the liquid fuel and obtain an optimal gaseous fuel/air mixture. Engine performance, efficiency and pollutant production strongly depend on the quality of the fuel/air mixture prior to combustion, and thus the details of the liquid-gas interface dynamics and atomization are of great importance.

Predicting the turbulent interface dynamics remains a challenging task for numerical simulations. Direct numerical simulations (DNS) have provided great insight for studying many aspects of turbulent immiscible interfaces. However, DNS must resolve all the relevant scales of motion, requiring enormous computational resources to simulate even simple geometries [1]. This requirement severely limits the range of resolvable time and spatial scales available to DNS and restricts DNS from being a viable tool for engineering design. A need therefore exists for alternative modeling approaches to predicting turbulent interface dynamics.

A number of models have been introduced to predict breakup, including stochastic models [2, 3] and interface transport equations for Reynoldsaveraged Navier-Stokes (RANS) equations [4]. The stochastic model requires a priori knowledge of the break-up mechanism for accurate predictions. Meanwhile the RANS approach models the mean interface density with a gradient diffusion-like hypothesis, which ignores the spatial grouping effects of liquid elements [1]. Many engineering applications of atomization, including aircraft engine combustors and diesel engine injectors can exhibit swirling flows, recirculation regions and jets in cross-flow or co-flow that are hard to predict using a RANS approach. Large-Eddy Simulations (LES) are often preferred in these applications, and therefore an atomization model consistent with the LES methodology is a desirable engineering design tool.

Several LES models for turbulent immiscible interfaces have been proposed in the past [5, 6]. These LES models, however, require the existence of a cas-

cade process to predict the unresolved scales, and furthermore require the dynamics of the unresolved scales to be inferred from the dynamics of the resolved scales. The LES methodology has proven to be remarkably successful in single phase turbulent flows due to the existence of the energy cascade. However, It remains unknown whether a similar cascade process can be taken advantage of to model the dynamics of turbulent immiscible interfaces and atomization. What's more, high resolution simulations of turbulent liquid jets show that small droplets can be ripped out from large ligaments in areas of high shear, circumventing any cascading process that a traditional LES approach would use [7].

Surface tension forces tend to increase at increasingly small length scales due to the smaller local radius of curvature, similar to the viscous forces responsible for the energy cascade. Although viscosity acts to dissipate kinetic energy at small scales, surface tension can either reduce surface corrugations or amplify them via an instability mechanism like Kelvin-Helmholtz, Rayleigh-Taylor or Rayleigh-Plateau. These instabilities all rely on sub-filter interface geometry to predict sub-filter corrugation growth, and thus require knowledge of the sub-filter interface geometry. Details of the sub-filter interface geometry are unavailable in the traditional LES approach, and therefore a dual-scale approach was proposed to provide a fully resolved realization of the sub-filter interface geometry [8] and properly handle the sub-filter effects. In this work a model is presented capable of predicting the effects of sub-filter shear-driven dynamics on the resolved interface geometry.

Governing Equations

The governing equations for the fully resolved motion of an unsteady, incompressible, immiscible, two-fluid system in the absence of surface tension and gravitational acceleration are the Navier-Stokes equations,

$$\frac{\partial \rho \mathbf{u}}{\partial t} + \nabla \cdot (\rho \mathbf{u} \otimes \mathbf{u}) = -\nabla p + \nabla \cdot (\mu (\nabla \mathbf{u} + \nabla^T \mathbf{u})),$$

$$\nabla \cdot \mathbf{u} = 0$$
(1)

where **u** is the fluid velocity, ρ is the density, p is the pressure, and μ is the dynamic viscosity. Surface tension and gravitational acceleration are neglected to focus on the shear driven instabilities of the interface. In addition to the momentum equation, the conservation of mass constrains the velocity field to be divergence-free. In the incompressible regime, fluid properties are taken to be uniform throughout each fluid. Therefore, ρ and μ are evaluated with a

volume-of-fluid scalar, ψ as,

$$\rho = \psi \rho_l + (1 - \psi) \rho_g, \qquad \mu = \psi \mu_l + (1 - \psi) \mu_g,$$
(2)

where the l and g subscripts denote properties in liquid and gas respectively. The volume-of-fluid scalar ψ is evaluated as $\psi=0$ in the gas and $\psi=1$ in the liquid. In addition ψ must also be transported with the flow field as,

$$\frac{\partial \psi}{\partial t} = -\mathbf{u} \cdot \nabla \psi = -\nabla \cdot (\mathbf{u}\psi) + \psi \nabla \cdot \mathbf{u}, \quad (3)$$

where the last term on the right-hand-side is zero for incompressible flows due to Eq. (1).

Filtered Governing Equations

Following the methodology of LES modeling, a spatial filter is applied to Eq. (1),

$$\frac{\partial \overline{\rho} \ \overline{\mathbf{u}}}{\partial t} + \nabla \cdot \left(\overline{\rho} \ \overline{\mathbf{u}} \otimes \overline{\mathbf{u}} \right) = -\nabla \overline{p} + \nabla \cdot \left(\overline{\mu} \left(\nabla \overline{\mathbf{u}} \otimes \nabla^T \overline{\mathbf{u}} \right) \right)$$

$$+ \boldsymbol{\tau}_1 + \nabla \cdot (\boldsymbol{\tau}_2 + \boldsymbol{\tau}_3),$$
 (4)

$$\nabla \cdot \overline{\mathbf{u}} = 0, \tag{5}$$

where the overbar $(\bar{*})$ implies spatial filtering, and

$$\boldsymbol{\tau}_1 = \frac{\partial \overline{\rho} \, \overline{\mathbf{u}}}{\partial t} - \frac{\partial \overline{\rho} \overline{\mathbf{u}}}{\partial t},\tag{6}$$

$$\boldsymbol{\tau}_2 = \overline{\rho} \ \overline{\mathbf{u}} \otimes \overline{\mathbf{u}} - \overline{\rho \mathbf{u} \otimes \mathbf{u}}, \tag{7}$$

$$\boldsymbol{\tau}_3 = \overline{\mu \left(\nabla \mathbf{u} + \nabla^T \mathbf{u} \right)} - \overline{\mu} \left(\nabla \overline{\mathbf{u}} + \nabla^T \overline{\mathbf{u}} \right), \quad (8)$$

where τ_1 , τ_2 and τ_3 represent the sub-filter effects due to acceleration, advection and viscosity respectively [5]. Applying the spatial filter to Eq. (2) yields

$$\overline{\rho} = \rho_l \overline{\psi} + \rho_g \left(1 - \overline{\psi} \right), \qquad \overline{\mu} = \mu_l \overline{\psi} + \mu_g \left(1 - \overline{\psi} \right).$$
(9)

The spatially filtered volume-of-fluid can be evaluated by solving

$$\frac{\partial \overline{\psi}}{\partial t} + \nabla \cdot \left(\overline{\mathbf{u}} \overline{\psi} \right) = \tau_{\psi}, \tag{10}$$

where τ_{ψ} is the sub-filter liquid flux and is obtained by applying the spatial filter to Eq. (3) and making use of Eq. (1).

$$\tau_{\psi} = \nabla \cdot \left(\overline{\mathbf{u}} \overline{\psi} - \overline{\mathbf{u}} \overline{\psi} \right) \tag{11}$$

The Dual-Scale Approach to Modeling Sub-Filter Shear-Induced Velocities

The classical LES modeling approach in singlephase flows assume the existence of a cascading process where there is a net transfer of energy to small scales. Applying a cascade process to the atomization process for a liquid jet for example, would imply that the jet first breaks up into large scale structures and then continues to break up into increasingly small-scale structures. However as mentioned previously, evidence from high-resolution simulations of atomizing liquid turbulent jets suggest that the atomization process does not follow a cascade process. These simulations show that small-scale drops can be ejected during the ligament-formation process, circumventing any cascade process for the phase interface geometry [7].

Instead of relying on a cascade process for the sub-filter motion, the dual-scale approach aims to maintain a fully resolved realization of the interface geometry at all times [8]. The dynamics of this interface are governed by Eq. (3), where $\bf u$ is the fully resolved fluid velocity. The fully resolved velocity is decomposed into its filtered $\bf \bar{u}$ and sub-filter $\bf u_{sg}$ components,

$$\mathbf{u} = \overline{\mathbf{u}} + \mathbf{u}_{sq},\tag{12}$$

which can then be substituted in Eq. (3) as

$$\frac{\partial \psi}{\partial t} = -\nabla \cdot ((\overline{\mathbf{u}} + \mathbf{u}_{sg}) \, \psi) + \psi \nabla \cdot (\overline{\mathbf{u}} + \mathbf{u}_{sg}) \,. \quad (13)$$

Finally, $\overline{\psi}$ in Eq. (9) can be evaluated by a direct explicit filter,

$$\overline{\psi} = \int \mathcal{G}(\mathbf{x})\psi d\mathbf{x}.$$
 (14)

where $\mathcal{G}(\mathbf{x})$ is a spatial filter function. With a model for \mathbf{u}_{sq} and making use of Eq. (14), there is no need to construct a model for τ_{ψ} , and Eq. (9) can be evaluated directly. What's more, the unclosed terms in the Navier-Stokes equations, $\boldsymbol{\tau}_1$, $\boldsymbol{\tau}_2$ and $\boldsymbol{\tau}_3$, can be calculated directly by first evaluating the fully resolved realization of ρ , μ , ψ and \mathbf{u} using Eqs. (2), (12) and (13), and then taking an explicit filter of the terms in Eqs. (6), (7) and (8). Finally, it is worth noting that because ρ and μ are uniform throughout each fluid, the terms τ_1 and τ_3 reduce to zero when the spatial filter does not contain an interface, and τ_2 reduces the standard sub-grid stress term that can be modeled by any classical single-phase LES technique. Therefore the dual-scale procedure needs only be applied in the vicinity of the interface.

The dual-scale method does present an exact closure of the sub-grid terms, however the modeling task is now shifted to maintaining a fully resolved realization of the interface geometry by solving Eq. (13) and modeling the sub-filter velocity

 \mathbf{u}_{sg} . A model for \mathbf{u}_{sg} is proposed consisting of four parts,

$$\mathbf{u}_{sg} = \mathbf{u}' + \delta \mathbf{u} + \mathbf{u}_{\sigma} + \mathbf{u}_{g} \tag{15}$$

where \mathbf{u}' , $\delta \mathbf{u}$, \mathbf{u}_{σ} and \mathbf{u}_{g} are the sub-filter velocities due to turbulent fluctuations, shear-induced instabilities, surface tension and acceleration instabilities respectively. Models for \mathbf{u}' and \mathbf{u}_{σ} are presented in [9] and [10] respectively, a model for $\delta \mathbf{u}$ is presented here and \mathbf{u}_{g} is the subject of future work.

Sub-Filter Velocity due to Shear-Induced Instabilities

To model the shear-induced sub-filter velocities, we consider the motion of the phase interface between two inviscid and incompressible fluids. This motion is governed by the Euler equations presented here in dimensionless form as

$$\frac{\partial \delta \mathbf{u}}{\partial t} + (\delta \mathbf{u} \cdot \nabla) \, \delta \mathbf{u} = -\frac{1}{\rho} \nabla p, \qquad \nabla \cdot \delta \mathbf{u} = 0, \quad (16)$$

where the velocity $\delta \mathbf{u}$ and density ρ are defined on either side of the phase interface Γ , and p is the pressure. Additionally, the boundary conditions at the interface are given by

$$[(\delta \mathbf{u}_g - \delta \mathbf{u}_l) \cdot \mathbf{n}] \Big|_{\Gamma} = 0, \tag{17}$$

$$\left[\mathbf{n} \times (\delta \mathbf{u}_g - \delta \mathbf{u}_l)\right]\Big|_{\Gamma} = \boldsymbol{\eta},\tag{18}$$

$$[p_g - p_l] \Big|_{\Gamma} = \frac{1}{We} \kappa, \tag{19}$$

and the velocities are constrained to $U_{\pm\infty}$ far from the interface. In these boundary conditions, ${\bf n}$ and ${\bf t}$ are unit-vectors normal and tangent to the interface, ${\boldsymbol \eta}$ is the vectorial vortex-sheet strength, $We = \rho_{\rm ref} L_{\rm ref} u_{\rm ref}^2/\sigma$ is the Weber number, σ is the surface tension coefficient, $\rho_{\rm ref}$, $u_{\rm ref}$ and $L_{\rm ref}$ are the reference density, velocity and length respectively, and κ is the local curvature of Γ . The evolution of the vortex sheet strength can be derived by introducing velocity potentials into the Euler equations and its accompanying boundary conditions to produce a vortex sheet transport equation [11, 12, 13, 14].

$$\begin{split} &\frac{\partial \boldsymbol{\eta}}{\partial t} + \delta \mathbf{u} \cdot \nabla \boldsymbol{\eta} = -\mathbf{n} \times \left[(\boldsymbol{\eta} \times \mathbf{n}) \cdot \nabla \delta \mathbf{u} \right] + \\ &\mathbf{n} \left[(\nabla \delta \mathbf{u} \cdot \mathbf{n}) \cdot \boldsymbol{\eta} \right] + \frac{1}{W_{\mathcal{C}}} \left(\mathbf{n} \times \nabla \kappa \right) \end{split} \tag{20}$$

The terms on the left-hand side of Eq. (20) represent the temporal changes and convective transport of the vortex sheet strength. The terms on the

right-hand side describe the stretching of the vortex sheet and surface tension effects. Note that η is a surface quantity so Eq. (20) only needs to be solved at the location of the interface. Finally, the self-induced velocities due to the presence of the vortex sheet can be evaluated via a vector potential ψ defined by

$$\nabla^2 \psi(\mathbf{x}) = \omega(\mathbf{x}),\tag{21}$$

where the vorticity ω can be evaluated from the redistributed η field from the following volume integral [13].

$$\omega(\mathbf{x}) = \int_{V} \eta(\mathbf{x}') \delta(\mathbf{x} - \mathbf{x}') \delta(G(\mathbf{x}')) |\nabla G(\mathbf{x}')| d\mathbf{x}'$$
(22)

In Eq. (22) δ is the dirac delta function and $G(\mathbf{x})$ is the Levelset function of the interface. Upon solving Eq. (21) with this vorticity, the velocity $\delta \mathbf{u}$ can be evaluated with

$$\delta \mathbf{u}(\mathbf{x}) = \int_{V} \delta(\mathbf{x} - \mathbf{x}') \left(\nabla \times \boldsymbol{\psi} \right) d\mathbf{x}'. \tag{23}$$

Finally, Eq. (3) and (20) are closed by the velocity calculated from Eq. (23) and thus form the system of equations that govern the dynamics of the phase interface Γ in the presence of surface tension forces.

Numerical Approach

The Navier-Stokes equations are solved using NGA, a structured, staggered, finite difference flow solver with a fractional step method [15]. The task of maintaining a fully resolved realization of the phase interface geometry is achieved by solving Eq. (13) on a high resolution auxiliary Cartesian grid independent of the underlying flow solver grid. The Refined Level Set Grid (RLSG) method [16] is used to manage the auxiliary grid and activate it in regions where the spatial filter contains an interface as illustrated in Fig. (1).

Eq. (13) is advanced using the unsplit geometric transport scheme of Owkes and Desjardins [17]. This method ensures that volume-of-fluid scalars remain bounded and that discrete volume is conserved for each fluid. The geometric interface within each computational cell of the RLSG is built using PLIC reconstruction with analytical formulas [18] and ELVIRA estimated normals [19]. Additionally, eq. (20) is advanced in time using a first Euler time

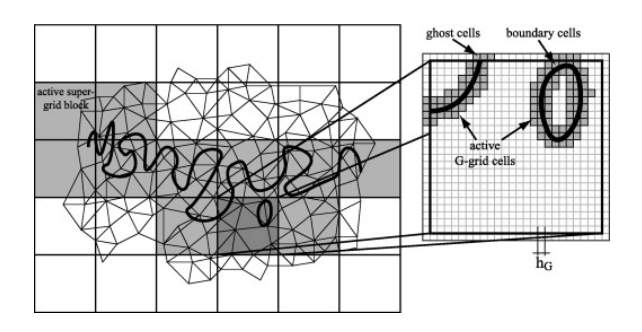


Figure 1: Refined Level Set Grid [16]

integration method and first order upwind scheme for the convective terms.

In order to evaluate the right hand side of the vector potential equation, Eq. (21), a vortex-in-cell approach is employed to evaluate the vorticity at each grid point in the computational domain. The vorticity at each grid point is calculated using a numerical version of Eq. (22) and an approximated, smooth delta function. This smooth delta function has the effect of spreading the vorticity, a quantity theoretically located only at the interface, to neighboring grid points. This approach is therefore similar in spirit to several vortex-in-cell methods that spread the vorticity of vortex particles to their surrounding grid points [20]. For the purpose of this paper the following delta function definitions will be used,

$$\delta(\mathbf{x} - \mathbf{x}') = \delta_{\epsilon}(x - x')\delta_{\epsilon}(y - y')\delta_{\epsilon}(z - z'), \quad (24)$$

$$\delta\left(G(\mathbf{x}')\right) = \delta_{\epsilon}(G(\mathbf{x}')),\tag{25}$$

and the following numerical delta function δ_{ϵ} [21]

$$\delta_{\epsilon}(x) = \begin{cases} \frac{1}{2\epsilon} \left[1 + \cos\left(\frac{\pi x}{\epsilon}\right) \right], & |x| \le \epsilon, \\ 0, & |x| > \epsilon. \end{cases}$$
 (26)

Integrating Eq. (22) numerically is started by first evaluating

$$\mathbf{\Omega}(\mathbf{x}',t) = \boldsymbol{\eta}(\mathbf{x}',t)\delta(G(\mathbf{x}'))|\nabla G(\mathbf{x}')| \qquad (27)$$

for all cells in the \mathcal{N} -band and then integrating

$$\omega(\mathbf{x},t) = \int_{V'} \delta(\mathbf{x} - \mathbf{x}') \Omega(\mathbf{x}',t) d\mathbf{x}' \qquad (28)$$

for all cells within the $\mathcal{N}-$ band with a midpoint rule. In Eq. (28), V' is the volume where $|x-x'| \leq \epsilon$,

 $|y-y'| \leq \epsilon$ and $|z-z'| \leq \epsilon$. The Poisson equation governing the vector potential, Eq. (21), is solved by the Aztec package found in the Trilinos software library [22]. The vector potential equation is solved throughout the entire computational domain on a staggered grid as proposed by Uchiyama et al. [23] and applying appropriate boundary conditions at the edges of the domain.

The shear-induced velocity, $\delta \mathbf{u}$, can then be computed from the vector potential in Eq. (23) in a two-step process. In the first step, an initial velocity \mathbf{U} is evaluated at cell faces using second-order central finite difference stencils on the edge-centered components of the vector potential $\boldsymbol{\psi}$. In order to maintain consistency with the numerical vorticity spreading in Eq. (28), the same numerical integration method and numerical δ function must be used in an interpolation step to calculate $\delta \mathbf{u}$,

$$\delta \mathbf{u}(\mathbf{x}, t) = \int_{V'} \delta(\mathbf{x} - \mathbf{x}') \mathbf{U}(\mathbf{x}', t) d\mathbf{x}', \qquad (29)$$

within the \mathcal{N} -band.

Results

The sub-filter velocity generation technique is tested with a desingularized version of the Moore singularity problem following Krasny [24]. The initial condition for the interface is given by

$$y(x, t = 0) = A_0 \sin\left(\frac{2\pi}{B} \left[x - A_0 \sin\frac{2\pi}{B}x\right]\right), (30)$$

where A_0 and B are the amplitude and wavelength of the disturbance respectively. The initial vortex sheet strength is then given by

$$\eta_z(\mathbf{x}, t = 0) = \frac{\eta_z^*}{\sqrt{1 + \frac{4\pi A_0}{B} \cos\frac{2\pi}{B}x + 2\left[\frac{2\pi A_0}{B} \cos\frac{2\pi}{B}x\right]^2}},$$
(31)

where η_z^{\star} is the unnormalized vortex sheet strength. For this test case the initial amplitude and wavelength are $A_0=0.01$ and B=1, and the unnormalized vortex sheet strength is $\eta_z^{\star}=-1$. The simulation will take place in a 1×1 domain with an equidistant 256×256 cartesian grid and periodic boundary conditions on the left and right walls.

The results in Fig. (2) show agreement with the results from the work of Krasny [24] in the outer core shape, however the number of turns generated in the inner core is noticeably different in later times. The lower number of turns in this study is due to the

vorticity calculation in Eq. (22). Because of the inclusion of the $\delta(G(\mathbf{x}))$, the method is unable to distinguish between closely spaced interface segments and only accounts for the closest interface. This can potentially underpredict vorticity in the central core and generate fewer turns than other desingularization methods like that of Krasny.

Additionally, to demonstrate the model's capability of simulating shear in a fully 3-dimensional case, the temporal evolution of a doubly periodic liquid interface is presented. The interface is perturbed by both a streamwise and spanwise disturbance. The shape of the initial interface is given by

$$G(\mathbf{x}, t = 0) = z - A_0 \sin\left(\frac{2\pi}{B_0} \left[x - A_0 \sin\frac{2\pi}{B_0}x\right]\right) - A_1 \sin\left(\frac{2\pi}{B_1}y\right). \tag{32}$$

where A_0 and B_0 are the amplitude and wavelength for the streamwise perturbation and A_1 and B_1 are the amplitude and wavelength for the spanwise perturbation. For this calculation both perturbations are of equal magnitude and thus $A_0 = A_1 = 0.01$ and different wavelengths, $B_0 = 1, B_1 = 1/2$. The only non-zero initial component of η is given by

$$\eta_y(\mathbf{x}, t = 0) = \frac{\eta_y^*}{\sqrt{1 + \frac{4\pi A_0}{B_0} \cos\frac{2\pi}{B_0} x + 2\left[\frac{2\pi A_0}{B_0} \cos\frac{2\pi}{B_0} x\right]^2}},$$
(33)

where $\eta_y^{\star}=1.$ The calculations are evaluated on a [0,1]x[0,1]x[-1.0,-1.0] domain employing a 64x64x128 equidistant Cartesian grid with periodic boundary conditions applied in the x and y directions and slip conditions applied on the top and bottom walls. Fig. (3) shows the results of the evolution of an interface perturbed by these conditions. As expected, the interface shows a strong roll-up feature in the streamwise direction and, interestingly, shows Rayleigh-Taylor like dynamics in the spanwise direction. Although density driven instabilities can be incorporated into the vortex sheet method, these effects are not active in this simulation and are not driving the behavior observed in Fig. (3). The effect seen here is due to the dilatation and stretching terms in Eq. (20) which are reorienting the vortex sheet strength from η_y to η_x . Since the spanwise perturbation is a pure sine wave, the reorientation of the vortex sheet strength "generates" vorticity in the same interface locations as the baroclinic torque term would. These Rayleigh-Taylor dynamics in doubly periodic shear layers have also been observed in past work conducted on vortex sheet methods [25].

Conclusions

In this paper a method to reconstruct sub-filter shear driven velocities for use in a Dual-Scale LES model has been presented. The method generates shear driven velocities by applying a vortex sheet at the interface location of a phase interface between a liquid and gas. The velocities induced by that vortex sheet can then be found by generating a vorticity field and solving the vector potential equation. These velocities are then used to transport the interface and vortex sheet strength. Finally, the updated interface geometry can be explicitly filtered and sent back to the underlying Navier-Stokes flow solver. The method has been tested against wellknown results and shows excellent agreement in capturing the motion of the interface under reasonable conditions.

Acknowledgements

We gratefully acknowledge NSF grant 1803657 for funding this research.

References

- [1] M. Gorokhovski and M. Herrmann. Annual Review of Fluid Mechanics, 40(1):343–366, 2008.
- [2] V. Sabel'nikov, M. Gorokhovski, and N. Baricault. Combustion Theory and Modelling, 10(1):155–169, 2006.
- [3] V. Sabel'nikov, A. Chtab, and M. Gorokhovski. In J.M.L.M. Palma and A. Silva Lopes, editors, Advances in Turbulence XI, pp. 209–211, Berlin, Heidelberg, 2007. Springer Berlin Heidelberg.
- [4] A. A. Burluka and R. Borghi. *Atomization and sprays*, 11(6), 2001.
- [5] A. Toutant, E. Labourasse, O. Lebaigue, and O. Simonin. Computers and Fluids, 37(7):877– 886, 2008.
- [6] E. Labourasse, D. Lacanette, A. Toutant, P. Lubin, S. Vincent, O. Lebaigue, J.-P. Caltagirone, and P. Sagaut. *International Journal* of Multiphase Flow, 33(1):1–39, 2007.
- [7] M. Herrmann. Volume 2: Combustion, Fuels and Emissions:455–464, 06 2009.
- [8] M. Herrmann and M. Gorokhovski. *Proceedings* of the Summer Program, pp. 171–181, 2008.

- [9] K. Dominic, J. Uglietta, and M. Herrmann. In M. Gorokhovski and F. S. Godeferd, editors, *Turbulent Cascades II*, pp. 257–264, Cham, 2019. Springer International Publishing.
- [10] M. Herrmann. Computers & Fluids, 87:92 101, 2013. USNCCM Moving Boundaries.
- [11] D. I. Pullin. Journal of Fluid Mechanics, 119:507532, 1982.
- [12] G. R. Baker, D. I. Meiron, and S. A. Orszag. Journal of Fluid Mechanics, 123:477–501, 1982.
- [13] M. Herrmann. Journal of Computational Physics, 203(2):539–571, 2005.
- [14] C. Pozrikidis. Journal of Fluid Mechanics, 425:335366, 2000.
- [15] O. Desjardins, V. Moureau, and H. Pitsch. *Journal of Computational Physics*, 227(18):8395 – 8416, 2008.
- [16] M. Herrmann. *Journal of Computational Physics*, 227(4):2674 2706, 2008.
- [17] M. Owkes and O. Desjardins. *Journal of Computational Physics*, 270:587 612, 2014.
- [18] R. Scardovelli and S. Zaleski. *Annual Review of Fluid Mechanics*, 31(1):567–603, 1999.
- [19] J. Pilliod and E. Puckett. *Journal of Computational Physics*, 199(2):465 502, 2004.
- [20] I.P Christiansen. Journal of Computational Physics, 13(3):363–379, 1973.
- [21] Charles S Peskin. Journal of computational physics, 25(3):220–252, 1977.
- [22] The Trilinos Project Team. The Trilinos Project Website.
- [23] Tomomi Uchiyama, Yutaro Yoshii, and Hirotaka Hamada. International Journal of Numerical Methods for Heat & Fluid Flow, 2014.
- [24] R. Krasny. Journal of Computational Physics, 65(2):292–313, 1986.
- [25] Mark Joseph Stock. PhD thesis, University of Michigan, 2006.

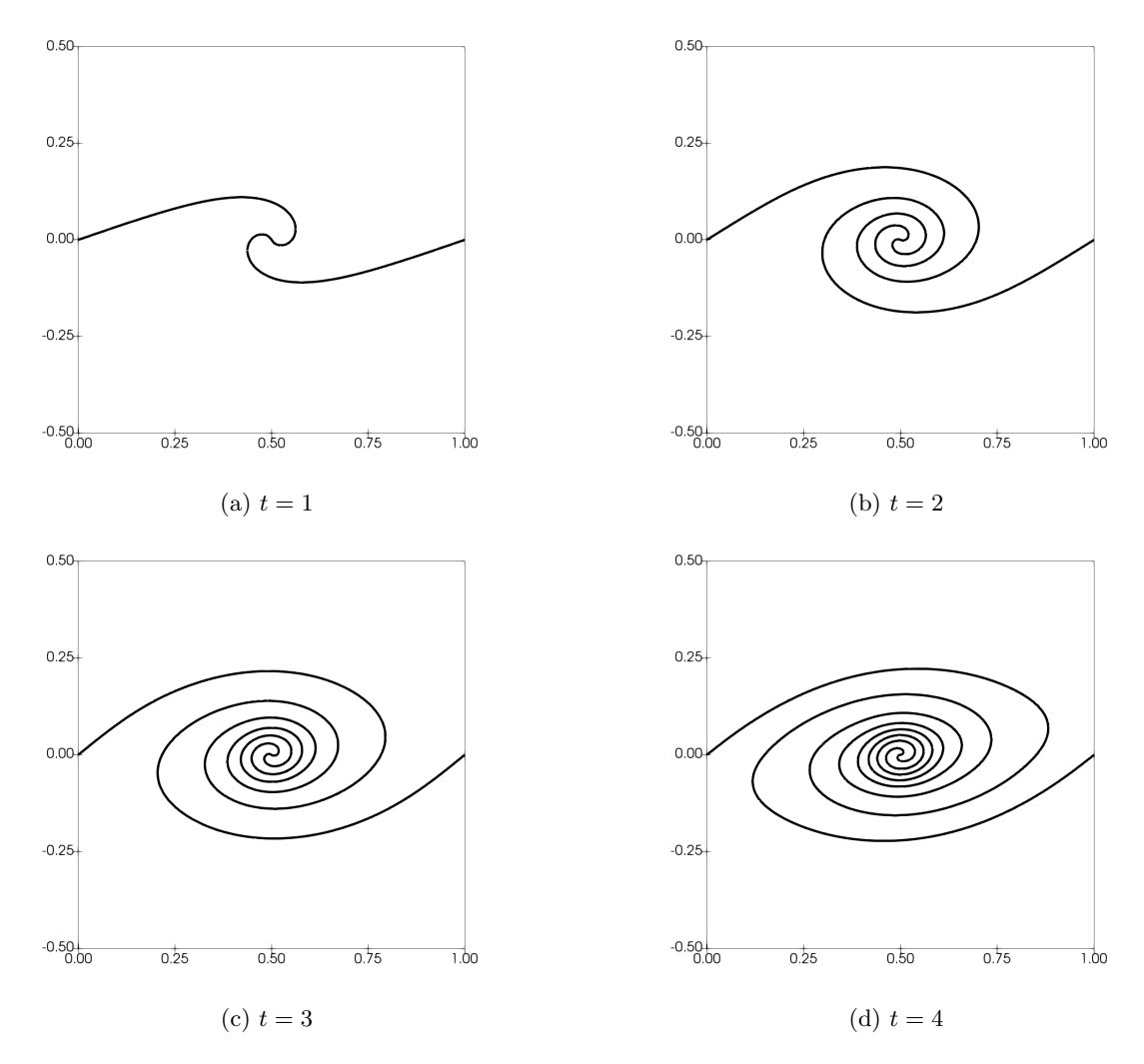


Figure 2: Interface shape, 256 x 256 grid, $\epsilon=16/256, t=1,2,3,4$

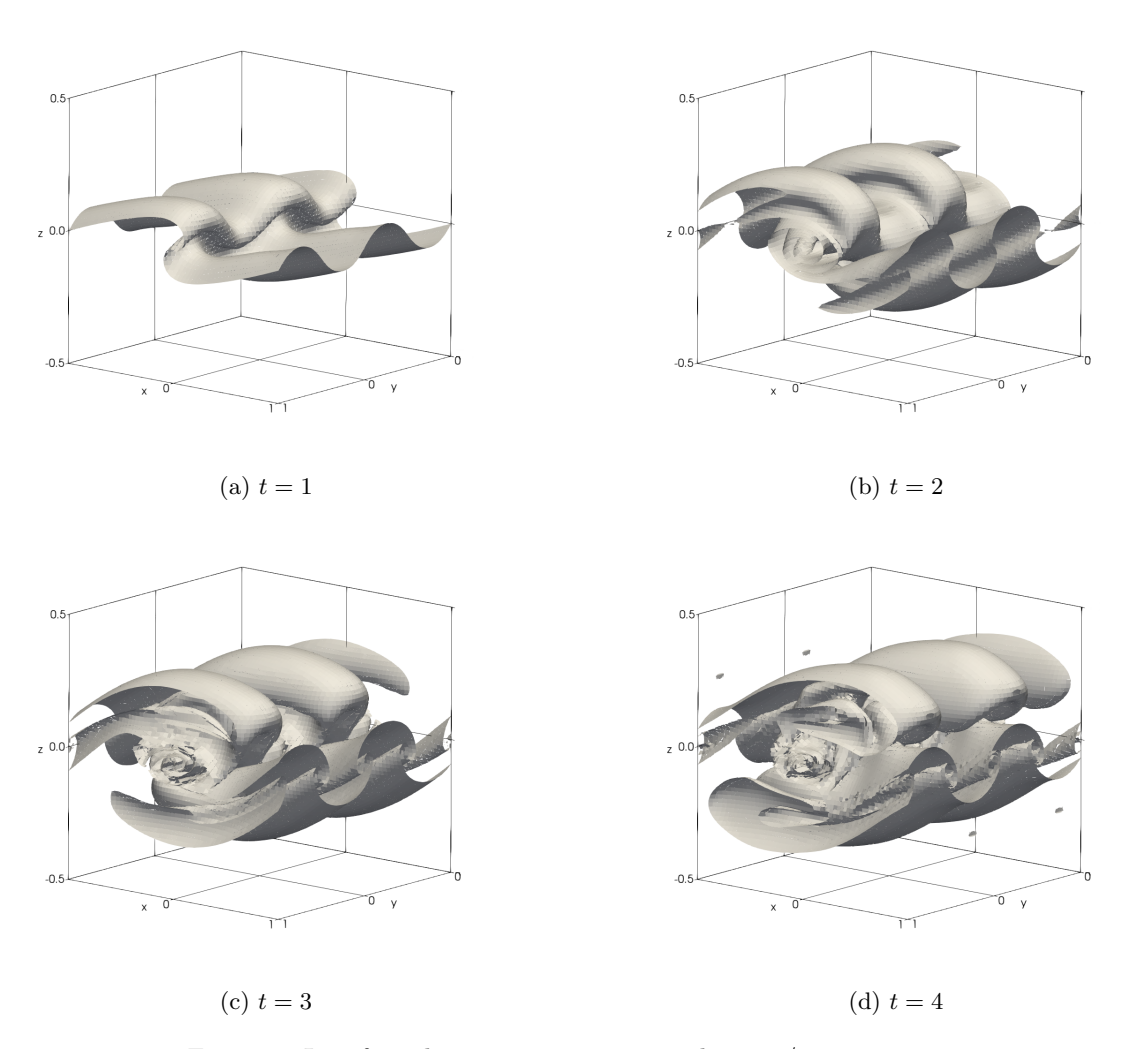


Figure 3: Interface shape, 64 x 64 x 128 grid, $\epsilon=4/64, t=1,2,3,4$